Wall-Layer Model for the Velocity Profile in Turbulent Flows

J. D. A. Walker*
Lehigh University, Bethlehem, Pennsylvania
D. E. Abbott†
University of Massachusetts at Amherst, Amherst, Massachusetts
R. K. Scharnhorst‡
McDonnell Aircraft Company, St. Louis, Missouri
and
Gilbert G. Weigand§
Sandia National Laboratories, Albuquerque, New Mexico

In the calculation of turbulent flows near walls, a substantial amount of mesh points and computational effort is required to adequately resolve the intense velocity profile variations in the near-wall region. In this study, a profile approximation is obtained for the mean velocity that is based upon consideration of the coherent structure of the time-dependent wall-layer flow. The profile approximation is an analytical formula that satisfies all of the required compatibility conditions at the wall and the logarithmic behavior at the edge of the wall layer. A general method for utilizing the present wall-layer profile model in a prediction method is indicated.

I. Introduction

RECENTLY there has been considerable interest in the development of wall functions to represent the mean velocity profile near the wall layer of a turbulent boundary layer. Here, the term "wall layer" is understood to denote the portion of the boundary layer from the wall to the overlap zone (where the mean velocity is logarithmic in distance normal to the wall). Wall-layer regions also occur in turbulent internal flows and, consequently, the capability to accurately predict wall-layer behavior is important in a wide variety of engineering applications. Because of the intense variation of the mean velocity profile in the wall layer, relatively large numbers of mesh points (as well as considerable computational effort) are required in prediction methods which attempt to compute the velocity profile all the way to the wall. The attraction of wall functions is the expectation that the velocity profile near the edge of the wall layer may be represented by some analytical expression (such as a form of the "law of the wall") at the first numerical mesh point from the wall, in part of a coarse mesh that adequately resolves the details of the effectively inviscid flow away from the wall. If such an approach can be developed and refined, the economies of mesh points and computational effort are substantial. Some work in this area has recently been reviewed by Rubesin and Viegas[1] where a number of approaches for patching an outer numerical solution to a wall function at the first point from the wall are critically discussed. In the present study, an analytical expression for the mean velocity profile throughout the wall layer is derived through a time-average of typical time-dependent observed coherent motions within the wall layer. The subsequent analysis of the time-dependent flow is complex, and the reasoning involves a number of subtle points; however, the final resulting time-mean profile is a relatively simple analytical expression that spans the entire wall layer from the wall to the logarithmic region. A general method for using this profile in a prediction method will also be briefly discussed in this paper.

As a result of over two decades of experimental work,[2-12] it has been possible to identify a repeatable and cyclic process in turbulent flows near walls; in this process, the wall layer is observed to grow slowly over a period of time and then interact strongly with the outer flow in an event usually referred to as bursting. The principal features of the wall-layer flow play a central role in the present analysis and are reviewed in Sec. II. The present approach is somewhat unconventional in that the analysis seeks to develop a model for the mean velocity profile rather than the Reynolds stress $-\overline{u'v'}$. Justification for the use of wall-layer profiles in a prediction method is provided by asymptotic analyses of the time-mean equations for large Reynolds numbers, originally due to Fendell[13] and Mellor[14]; the central results are quoted in Sec. III. The present analysis seeks to construct the particular time-dependent motions which average to produce the major contributions to the mean velocity profile; it is necessary to restrict attention (in the analysis) to motions that produce contributions to the mean quantities that have orders of magnitude compatible with established asymptotic results,[13-16] and which are consistent with observed trends for Reynolds stress $-\overline{u'v'}$ and the turbulence intensities $\overline{u'^2}$, $\overline{v'^2}$, and $\overline{w'^2}$. A model of the time-dependent flow is considered in Sec. IV; possible similarity solutions are discussed in Sec. V, and an expression for the mean profile is obtained in Sec. VI. Finally, the potential application of the present profiles in a general prediction method is described in Sec. VII.

II. Experimental Background

Since the original observations[2] of the cyclic behavior of turbulent wall-layer flow, a large number of experimental studies have clearly established the general nature of the processes involved.[5,8] Although a variety of questions concerning

Presented as Paper 86-0213 at the AIAA 24th Aerospace Sciences Meeting, Reno, NV, Jan. 6-9, 1986; received July 18, 1986; revision received May 28, 1988.

*Professor, Department of Mechanical Engineering and Mechanics. Member AIAA.
†Associate Vice Chancellor for Computing and Information Systems. Member AIAA.
‡Lead Engineer. Member AIAA.
§Supervisor, Parallel Processing Division.

the causes and effects of the observed phenomena are not yet fully resolved, it is possible to put together a general descriptive account. There are two main features that are known to dominate the dynamics of the wall-layer flow, and these are the wall-layer streaks and the bursting phenomenon. If observations are carried out over a fixed area of the wall, the wall layer will be seen to be in a quiescent[2] state for a large majority of the total observation time. During the quiescent period, the wall-layer streaks are observed when a visualization medium such as dye or hydrogen bubbles is introduced into the wall-layer flow. The markers are observed to collect into relatively long streaks that are essentially aligned in the streamwise direction. The streaks are separated by an average spanwise distance[2,5,9] of 100 ν/u_τ, where ν is the kinematic viscosity and u_τ is the local mean friction velocity; the streaks are elongated in the streamwise direction, and typically may have a length on the order of 1000 ν/u_τ. The streamwise velocity in the vicinity of the streaks is generally less than that of the mean profile, and thus the terminology "low-speed streaks" is common. The cause of the wall-layer streaks is not generally agreed upon, but it is reasonable to suppose that the streaks are the signature of vortices (probably of the hairpin type[17-19]) which are being convected over the wall within the boundary layer but above the streaks.

Although the observed portion of the wall layer is in the quiescent state, the time-dependent flow in the turbulent boundary layer may be considered to have a distinct double structure; i.e., there is a well-defined inner wall layer and an outer layer. The wall layer is very thin with respect to the outer layer; furthermore, at this stage the wall layer only responds passively to events that are taking place in the outer layer (such as the passage of hairpin vortices). Put in another way, there are no strong interactions between the inner and outer regions during the quiescent period. It is worthwhile to remark that the boundary between the two regions is not distinct or static at some value of $y^+ = yu_\tau/\nu$, where y measures distance normal to the wall; rather, the boundary is to be regarded as continuously in motion as the cycle progresses. The quiescent period is generally observed to initiate with the "sweep," which is characterized[4] by a penetration of high-speed fluid from the outer region of the boundary layer toward the wall; in the latter stages of the sweep event, the wall-layer streaks appear. At this stage the wall layer is very thin. There then ensues a relatively long quiescent period in which there are no major interactions with the outer flow, and the wall layer continuously thickens due to viscous diffusion.

The quiescent period is observed to terminate at isolated spanwise and streamwise locations in the bursting process. The phenomenon is normally associated with a wall-layer streak; initially, the low-speed streak lifts away[3] from the wall, and oscillations in both the spanwise and normal directions are observed. The oscillations appear to increase in amplitude and scale until a breakdown occurs in the form of a chaotic eruption of wall-layer fluid into the outer layer. The ejection of wall-layer fluid is soon followed by a sweep[4] of outer-layer fluid toward the wall; in the process, the chaotic motion due to the burst is swept away. At this stage the wall-layer streaks re-appear, but now at different spanwise locations, and a new quiescent period begins; over a large number of cycles, the spanwise distribution of the streaks is random. The cause of the bursting phenomenon is not generally agreed upon; however, the observed phenomena is probably due to the action of convected hairpin vortices. It is known that moving vortices[20-24] induce a region of adverse pressure gradient on the viscous flow near a wall, and that this soon actuates an unsteady separation effect; in many situations this leads to the evolution of secondary vortices and a strong viscous-inviscid interaction in the form of an eruption of the viscous flow near the wall. The bursting phenomenon bears a strong resemblance to known vortex-induced eruptions.[20,21,24] However, even if causal questions are set aside for the moment, it is clear that the bursting phenomenon represents a local breakdown of a hitherto relatively well-ordered wall-layer flow. Consequently, it is a brief period when the wall layer and the outer layer of the boundary layer interact strongly in what may be characterized as an unsteady viscous-inviscid interaction. For a fixed observation area of the wall, let T_q denote the average duration of the quiescent period (measuring a period from the latter stages of the sweep to the onset of the bursting phenomenon); in addition, let T_e be the average duration of the bursting process or localized breakdown of the wall-layer flow. The average period between bursts is the sum $T_B = T_q + T_e$, and it is generally observed[2,3,5] that $T_q \gg T_e$. Consequently, the time associated with the breakdown and interaction is brief with respect to that of the quiescent period. However, the majority of Reynolds stress production occurs during these brief periods of breakdown[3,5,8] and not during the quiescent period. The bursting process is the fundamental regenerative mechanism of production in which new vorticity from the wall-layer region is abruptly and intermittently introduced into the outer regions of the turbulent boundary layer. Thus, if direct modeling of Reynolds stress $-\overline{u'v'}$ near a wall is contemplated, it is evident that an analysis of a typical bursting process is necessary if the model is to reflect the true physics of the flow. Unfortunately, the observed strong interaction that occurs is complex and difficult to treat on a theoretical basis. The alternate approach considered in the present paper is to focus on the development of the mean velocity profile in the wall layer. In view of the relatively long duration, the vast majority of contributions to the mean profile (recorded by a probe, for example) are made during the quiescent period when the wall-layer flow is reasonably well ordered, and when no strong interactions occur between the wall layer and the outer flow.

III. Time-Mean Structure

The analysis is carried out in the limit of large Reynolds numbers with the objective of isolating the dominant terms in the governing equations; the results are expected to be asymptotic for finite but large Reynolds numbers. It is worthwhile at this stage to review the known features[13-16] of the time-mean asymptotic structure. Consider a nominally steady two-dimensional turbulent boundary-layer flow, and let (x,y) measure distances in the streamwise direction and normal to the wall, respectively; the corresponding mean velocity components are $(\bar{u},\bar{v})$, and $u_e(x)$ denotes the mainstream velocity. Let $Re = U_0 L/\nu$ denote the Reynolds number based on a representative length L and speed U_0; in the limit $Re \to \infty$, the important small parameter[13,14] is the dimensionless friction velocity defined by

$$u_* = u_\tau(x,Re)/u_e(x) \tag{1}$$

It can be shown[13-16] that $u_* \to 0$ as $Re \to \infty$ and, in addition, there is a self-consistent two-layer structure associated with the boundary-layer solution. In the outer layer, the streamwise velocity is a perturbation about the mainstream, and the Reynolds stress is $0(u_\tau^2)$, viz.,

$$\bar{u} = u_e(x)[1 + u_* U_1(x,\eta) + \ldots], \quad \overline{u'v'} = -u_\tau^2 \Sigma_1(x,\eta) + \ldots \tag{2}$$

Here $\eta = y/\Delta_0$ is the scaled outer variable; Δ_0 is representative of the outer-layer thickness and is $0(u_*)$. The function Σ_1 is arbitrary, and in order to define a specific outer-layer turbulence model, some functional form must be specified relating Σ_1 to U_1. Upon substituting Eqs. (2) into the boundary-layer equations and neglecting terms $0(u_*)$, a simple differential equation for the defect function U_1 is obtained[13-16]; in a prediction method, this outer-layer equation would generally be solved numerically for U_1 (for a given turbulence model Σ_1)

subject to the conditions

$$U_1 \sim (1/\kappa)\log\eta + C_0(x) \text{ as } \eta\to 0, \qquad U_1\to 0 \text{ as } \eta\to\infty \quad (3)$$

Here κ is the von Kármán constant, which is usually assumed to have a value of $\kappa = 0.41$; the quantity $C_0(x)$ generally depends on the turbulence model used and must be calculated as part of the outer-layer numerical solution.

The main results in this paper concern the wall layer, and here the expressions for mean velocity and Reynolds stress are[13-16]

$$\bar{u} = u_\tau U^+ \ldots, \qquad -\overline{u'v'} = u_\tau^2\sigma_1(x,y^+) + \ldots \quad (4)$$

where the scaled inner variable $y^+ = u_\tau y/\nu$. To leading order, the equation governing the mean wall-layer flow[13-16] is

$$\frac{\partial^2 U^+}{\partial y^{+2}} + \frac{\partial\sigma_1}{\partial y^+} = p^+ \quad (5)$$

Here the pressure gradient parameter p^+ is defined by

$$p^+ = \frac{\nu}{\rho u_\tau^3}\frac{dp_e}{dx} \quad (6)$$

where $p_e(x)$ denotes the mainstream pressure. The important aspects of Eq. (5) are that 1) the convective terms are negligible to leading order, and the mean wall-layer flow arises from a balance between the Reynolds stress and viscous terms (in the limit $Re\to\infty$), 2) an x dependence can only occur in the wall-layer solution parametrically through matching to the outer-layer solution (as $y^+\to\infty$), and 3) if either of U^+ or σ_1 is known, the other function may be obtained from Eq. (5) by integration from the wall. Consequently, in regard to a wall-layer turbulence model, it is possible to model either the Reynolds stress *or* the mean profile; the former approach is conventional, but in this study it is the mean profile that will be modeled.

At the edge of the wall layer, the profile function U^+ must behave according to[13-16]

$$U^+ \sim (1/\kappa)\log y^+ + C_i \text{ as } y^+\to\infty \quad (7)$$

where C_i is a constant that is often assumed to have a universal value of 5.0. At the wall, it follows from the definition of $u_\tau = \sqrt{\tau_w/\rho}$ that

$$\frac{\partial U^+}{\partial y^+} = 1 \text{ at } y^+ = 0 \quad (8)$$

Here, τ_w is the wall shear, and ρ is the fluid density. In addition, the mean profile must satisfy certain wall compatibility conditions, which follow from a Taylor-series expansion for small y^+ of each of the terms in Eq. (5) and the fact that $\overline{u'v'}$ is $0(y^{+3})$ as $y^+\to 0$; it is easily shown that

$$\frac{\partial^2 U^+}{\partial y^{+2}} = p^+, \qquad \frac{\partial^3 U^+}{\partial y^{+3}} = 0 \text{ at } y^+ = 0 \quad (9)$$

Two other points are worthy of note. First, the mean normal velocity in the wall layer[13-16] is small, and $\bar{v} = 0(Re^{-1})$. The second point is that matching of the inner- and outer-layer velocities takes place with $y^+\to\infty$ and $\eta\to 0$; using Eqs. (3) and (7), it is easily verified[13,14] that

$$\frac{1}{u_*} = \frac{1}{\kappa}\log\left[\frac{\Delta_0 u_e u_*}{\nu}\right] + C_i - C_0(x) \quad (10)$$

This relation will be termed the match condition; it is a general result that is independent of any turbulence model and which relates the dimensionless friction velocity u_* to the outer-length scale Δ_0 and the inner and outer "log-law" parameters C_i and C_0, respectively. Note that to leading order, Eq. (10) indicates that $u_* \sim \kappa/\log Re_\delta$ as $Re\to\infty$, where Re_δ is a Reynolds number based on local boundary-layer thickness.

IV. Formulation of the Wall-Layer Problem

In this section, the equations governing the unsteady flow in the wall layer during the quiescent period are obtained as a subset of the full Navier-Stokes equations, with the objective of considering the flow evolution during a typical quiescent period. Let (x,y,z) measure distances in the streamwise, normal, and spanwise directions, respectively, with corresponding velocities (u,v,w). It is well established from experiment that the turbulent intensities $\overline{u'^2}$, $\overline{v'^2}$, and $\overline{w'^2}$ and the Reynolds stress $-\overline{u'v'}$ are $0(u_\tau^2)$ in the wall layer, and this suggests that the following scaled instantaneous velocities are appropriate during the quiescent period.

$$u^+ = u/u_\tau, \qquad v^+ = v/u_\tau, \qquad w^+ = w/u_\tau \quad (11)$$

It is assumed that the dimensions associated with typical motions are comparable in the normal and spanwise directions (and comparable to the mean wall-layer thickness); however, variations in the streamwise direction are considered to be less important, in view of the long length of the streaks relative to their spacing. It is also evident that the flow is unsteady and, therefore, the following scaled coordinates are introduced:

$$\tilde{x} = x/L_x, \qquad y^+ = yu_\tau/\nu, \qquad z^+ = zu_\tau/\nu, \qquad t^+ = u_\tau^2 t/\nu \quad (12)$$

Here L_x is a characteristic length in the x direction that is not known, but is expected to be associated with the streamwise extent of the outer-region structures responsible for the creation and evolution of the wall-layer streaks; recent evidence[17,18] indicates that these are convected hairpin vortices. In any event it is assumed, in accordance with experiment, that

$$L_x \gg \nu/u_\tau \quad (13)$$

It is noted in passing that in the early visual measurements of the time between bursts,[2] the burst period was considered to scale on inner variables; in subsequent years, probe measurements seemed to imply a dependence on outer variables,[5] and for a time the scaling was somewhat controversial. In recent times, visual investigations and probe studies[7,10-12] have supported a scaling based upon inner variables and, generally, indicate a period between bursts of $T_B^+ \simeq 100$. In the present context, the time scale is fixed by the requirement that the unsteady terms balance the viscous terms in the Navier-Stokes equations, since any other balance during the quiescent period leads to a contradiction.

The pressure in the wall layer may be expanded according to

$$p(x,t) = p_e(x) + (\rho u_\tau^3 L_x/\nu)p_0(\tilde{x},t^+) + \rho u_\tau^2 p_1(\tilde{x},y^+,z^+,t^+) + \ldots \quad (14)$$

where $p_e(x)$ is the mainstream pressure distribution. The pressure p_0 is an unsteady pressure variation that is impressed across the wall layer during the quiescent period, and which may be thought of as due to the motion of convected disturbances in the outer region (such as hairpin vortices); it is easily verified, upon substitution in the Navier-Stokes equations, that p_0 is independent of y^+ and z^+ as indicated in Eq. (14). The term p_1 is associated with the relatively organized motion between the streaks during the quiescent period. Upon substitution of Eqs. (11-14) into the unsteady Navier-Stokes equations, the following leading-order equations are obtained:

$$\frac{\partial u^+}{\partial t^+} + v^+\frac{\partial u^+}{\partial y^+} + w^+\frac{\partial u^+}{\partial z^+} = -p^+ - \frac{\partial p_0}{\partial\tilde{x}} + \frac{\partial^2 u^+}{\partial y^{+2}} + \frac{\partial^2 u^+}{\partial z^{+2}} \quad (15)$$

$$\frac{\partial v^+}{\partial t^+} + v^+\frac{\partial v^+}{\partial y^+} + w^+\frac{\partial v^+}{\partial z^+} = -\frac{\partial p_1}{\partial y^+} + \frac{\partial^2 v^+}{\partial y^{+2}} + \frac{\partial^2 v^+}{\partial z^{+2}} \quad (16)$$

$$\frac{\partial w^+}{\partial t^+} + v^+\frac{\partial w^+}{\partial y^+} + w^+\frac{\partial w^+}{\partial z^+} = -\frac{\partial p_1}{\partial z^+} + \frac{\partial^2 w^+}{\partial y^{+2}} + \frac{\partial^2 w^+}{\partial z^{+2}} \quad (17)$$

$$\frac{\partial v^+}{\partial y^+} + \frac{\partial w^+}{\partial z^+} = 0 \quad (18)$$

A similar set of equations has been considered by Chapman and Kuhn.[25] Here, p^+ is the mainstream pressure gradient defined by Eq. (6), which is small in most situations and here is assumed to be at most 0(1).

The objective now is to consider solutions of Eqs. (15–18), which correspond to representative motions during a typical quiescent state. The presence of the wall-layer streaks indicates that there are planes at certain spanwise locations that on average are aligned in the streamwise direction and across which there is no spanwise flow. Consider, therefore, the flow development between a typical pair of wall-layer streaks located at $z^+ = 0$ and $z^+ = \lambda^+$; here $\lambda^+ = \lambda u_\tau/\nu$, where λ is the mean streak spacing and λ^+ is generally observed[9] to have an average value of about 100. Since w^+ must vanish at $z^+ = 0$ and $z^+ = \lambda^+$ and in view of Eq. (18), it is possible to write v^+ and w^+ during a typical quiescent period according to

$$w^+ = -\sum_{n=1}^{\infty} \frac{\partial f_n}{\partial y^+} \sin\left(\frac{2n\pi z^+}{\lambda^+}\right)$$

$$v^+ = \frac{2\pi}{\lambda^+}\sum_{n=1}^{\infty} n f_n \cos\left(\frac{2n\pi z^+}{\lambda^+}\right) \quad (19)$$

Here $f_n(y^+,t^+)$ are the functional coefficients of the Fourier series, which are to be determined subject to the boundary conditions at the wall

$$f_n = \frac{\partial f_n}{\partial y^+} = 0 \text{ at } y^+ = 0 \quad (20)$$

A variety of different conditions could be considered for the asymptotic behavior of the instantaneous flow in the outer regions of the wall layer subject to the restriction that $w^+ = 0(1)$ as $y^+ \to \infty$; this is necessary since the motions represented by Eqs. (19) will make significant contributions to the turbulence intensities, and measurements show that $\overline{w'^2}/u_\tau^2$ is at most 0(1) for large y^+. The simplest outer condition that will produce the observed type of wall-layer structure, corresponding to the situation depicted schematically in Fig. 1, is obtained for

$$\frac{\partial f_1}{\partial y^+} \to W_1, \qquad \frac{\partial f_n}{\partial y^+} \to 0, \qquad n > 1 \quad (21)$$

as $y^+ \to \infty$. This is similar to the type of flow induced on the wall layer from above by a convecting hairpin vortex.[19] It is evident that the solution of Eqs. (16–18) develops independently from that of Eq. (15); by eliminating the pressure p_1, an equation describing the evolution of streamwise vorticity ζ_x^+ is obtained, viz.,

$$\frac{\partial \zeta_x^+}{\partial t^+} + v^+\frac{\partial \zeta_x^+}{\partial y^+} + w^+\frac{\partial \zeta_x^+}{\partial z^+} = \frac{\partial^2 \zeta_x^+}{\partial y^{+2}} + \frac{\partial^2 \zeta_x^+}{\partial z^{+2}} \quad (22)$$

Here,

$$\zeta_x^+ = \frac{\partial w^+}{\partial y^+} - \frac{\partial v^+}{\partial z^+} = -\sum_{n=1}^{\infty} g_n(y^+,t^+) \sin\left(\frac{2n\pi z^+}{\lambda^+}\right) \quad (23)$$

where the vorticity functions g_n are related to the f_n by

$$g_n(y^+,t^+) = \frac{\partial^2 f_n}{\partial y^{+2}} - \left(\frac{2n\pi}{\lambda^+}\right)^2 f_n \quad (24)$$

A sequence of equations for the g_n is readily obtained from Eq. (22) using standard methods,[26] and this set describes the evolving flow in the crossflow plane.

There are two major influences on the development of the streamwise velocity u^+, namely the nature of the outer streamwise flow imposed on the wall layer during the quiescent period, and the effect of the evolving flow in the crossflow plane that enters through the convective terms in Eq. (15). It may be verified upon substitution of Eqs. (19) into Eq. (15) that solutions for u^+ (which are symmetric about $z^+ = 0$) may be written

$$u^+ = u_0(y^+,t^+) + \sum_{n=1}^{\infty} u_n(y^+,t^+) \cos\left(\frac{2n\pi z^+}{\lambda^+}\right) \quad (25)$$

A variation in $\tilde{x}$ has not been written explicitly in this equation, since the dependence on $\tilde{x}$ is at most parametric (entering from the outer conditions for u^+ as $y^+ \to \infty$). Using standard methods for orthogonal functions,[26] it is readily shown that

$$\frac{\partial u_n}{\partial t^+} + \frac{2\pi n}{\lambda^+} f_n \frac{\partial u_0}{\partial y^+} + \frac{\pi}{\lambda^+}\sum_{m=1}^{\infty}\left\{\frac{\partial u_m}{\partial y^+}(j f_j + (n+m) f_{n+m}) + m\, u_m\left[\mathrm{sgn}(m-n)\frac{\partial f_j}{\partial y^+} + \frac{\partial f_{n+m}}{\partial y^+}\right]\right\} = \frac{\partial^2 u_n}{\partial y^{+2}} - \left(\frac{2n\pi}{\lambda^+}\right)^2 u_n \quad (26)$$

for $n = 1,2,3,\ldots$ and with $j = |m - n|$. The equation for u_0 is

$$\frac{\partial u_0}{\partial y^+} = -p^+ + \frac{\partial^2 u_0}{\partial y^{+2}} + M(y^+,t^+) \quad (27)$$

where

$$M = -\frac{\partial p_0}{\partial \tilde{x}} - \frac{\pi}{\lambda^+}\sum_{m=1}^{\infty} m \frac{\partial}{\partial y^+}(u_m f_m) \quad (28)$$

The set of Eqs. (22), (26), and (27) is a coupled system of nonlinear equations that can be solved numerically for an assumed initial velocity at the beginning of the quiescent period (the latter stages of the sweep). The full numerical problem has been considered by Walker and Herzog[27]; the main focus in this paper is to obtain an expression for the mean profile. At the same time, it is worthwhile to make two comments. First, there will be no net contribution to an average value of either w or v from the time-dependent motions represented by Eqs. (19); in addition, the first term in Eq. (25) (that is independent z^+) produces the principal contributions to the mean profile U^+ in the wall layer during the quiescent period. This is because after each wall-layer breakdown and subsequent sweep, the low-speed streaks appear at different spanwise locations; over a large number of cycles, the spanwise distribution of the streaks must be random. In the present analysis, an estimate of average quantities may be obtained by integration across the span from $z^+ = 0$ to λ^+, and in particular integration of Eqs. (19) yields zero; this is consistent with the known mean results that $\bar{w} = 0$ and $\bar{v}$ is small and $0(Re^{-1})$. Note, however, that the motions represented by Eqs. (19) and (25) do produce contributions to $\overline{u'^2}$, $\overline{v'^2}$, and $\overline{w'^2}$, which generally have an order of magnitude consistent with experiment. The second point is associated with the nature of the events that leads to the ultimate breakdown and destruction of the structure depicted schematically in Fig. 1. Walker and Herzog[27] have obtained numerical solutions for the developing

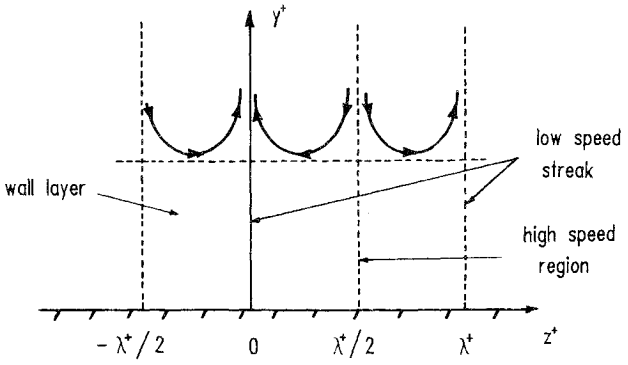

Fig. 1 Schematic diagram of average wall-layer structure during the quiescent state.

flow in the crossflow plane, and have shown that there are at least two routes to breakdown and eruption of the wall-layer flow. The evolution of the wall-layer flow depends on the value of a characteristic Reynolds number $Re_\lambda = W_1\lambda^+$. Here W_1 represents an average spanwise velocity at the wall-layer edge. In Eqs. (21), W_1 is associated with the first term in the Fourier series; however, more general situations could be considered in which all terms in the Fourier series for w^+ asymptote nonzero values as $y^+ \to \infty$. Measured values of $\overline{w'^2}$ for large y^+ suggest that a typical value of W_1 is about 2 and since $\lambda^+ \simeq 100$, Re_λ is, in general, large. Walker and Herzog[27] have considered solutions for the limit problem $Re_\lambda \to \infty$ and for finite values of Re_λ, and show that breakdown occurs through essentially the same fundamental mechanisms identified by Ersoy and Walker.[23] In the region near $z^+ = 0$, the outflow depicted in Fig. 1 gives rise to an adverse pressure gradient which is imposed on the viscous flow near the wall; ultimately, separation and regions of reversed flow develop in the crossflow plane near the wall. In the limit problem $Re_\lambda \to \infty$, and for a range of finite but high values of Re_λ, the crossflow plane separation quickly leads to a strong unsteady interaction of the wall-layer flow in the form of an eruption of the motion in the crossflow plane. As Re_λ decreases, the tendency for the crossflow plane solution to become eruptive gradually diminishes, and eventually the motion in the y^+z^+ plane evolves to an apparently steady state; however, in such cases, the streamwise velocity profiles were observed to develop a strong inflectional character in a region directly associated with the recirculating flow in the crossflow plane.[27] The latter situation is expected to be highly unstable and lead to a local rollover and interaction with the outer flow. Consequently, for sufficiently large values of the average spanwise velocity W_1 at the wall-layer edge, the structure in Fig. 1 and the problem defined by Eqs. (21), (22), (26), and (27) is inherently unstable, and the wall-layer flow must break down and interact strongly with the outer flow at finite values of t^+, which are 0(100).

V. The Similarity Solutions

Lasting contributions to the mean wall-layer profile during the quiescent period are associated with the u_0 component, which is governed by the diffusion Eq. (27). The forcing function M contains a pressure gradient term and terms arising from the evolution of the other streamwise modes; numerical solutions[27] indicate that for large Re_λ, the coupling between the solutions of Eqs. (26) and (27) is weak and, thus, this effect will be neglected here. The pressure $p_0(\tilde{x},t^+)$ is impressed across the wall layer and arises from the time-dependent motions in the outer region above the wall layer. A variety of forms are possible, corresponding to different types of convected disturbances. Alternatively, in the Van Driest[28] model of wall-layer turbulence, the motion considered is a Stokes flow driven by periodic velocity fluctuations at the wall-layer edge; this is obtained in the present context by taking $\partial p_0/\partial\tilde{x}$ equal to a periodic oscillatory function. However, it is evident that oscillatory solutions cannot make a net contribution to the mean profile and, thus, are not of interest. A class of solutions of Eq. (27) that do produce net contributions to the mean profile are similarity solutions corresponding to the relatively organized motion between streaks. These types of time-dependent solutions were originally studied by Einstein and Li[29] and Hanratty,[30] who neglected convection and considered a one-dimensional unsteady flow; these assumptions lead to a diffusion equation for the streamwise velocity. A uniform flow profile was assumed to initiate the cycle, and an error function solution describing a thickening diffusive flow was obtained.[29,30] A time-average over the assumed growth period yields an expression for the mean profile in the wall layer, but the profile is not logarithmic for large y^+. Subsequently, Black[31] considered an initial profile having a logarithmic behavior; his time-averaged solution is logarithmic for large y^+, although the treatment of the initial conditions gives rise to unacceptable irregularities in the mean profile. In Black's[31] theory of wall-layer turbulence, it was envisaged that an ordered array of unknown entities convects downstream at some characteristic velocity and causes unstable conditions to occur in the wall-layer flow. Some of the basic features of Black's model[31] are relevant to wall-layer turbulence[17-19,32]; however, the model has often been criticized for its great simplification and apparent failure to account for three-dimensional and nonlinear effects. In the present formulation, the role of the three-dimensional motion is evident in Eqs. (19), (22), (26), and (27); furthermore, the wall-layer flow is ultimately driven toward eruption via the inherent nonlinear behavior in Eqs. (22), (26), and (27).

In the present analysis, all relevant similarity solutions of Eq. (27) will be addressed. Consider first the homogeneous equation

$$\frac{\partial u_0}{\partial t^+} = \frac{\partial^2 u_0}{\partial y^{+2}} \tag{29}$$

and define the general similarity variables

$$\eta = y^+/2(t^+ + t_0^+)^{1/2}, \qquad \tau = t^+ + t_0^+ \tag{30}$$

Here t_0^+ is an undetermined constant at this stage which is introduced because of an uncertainty in the origin of time; the role of t_0^+ will be made clear subsequently. A sufficiently general similarity solution of Eq. (29) satisfying the no-slip condition is of the form

$$u_0 = g(\eta)h(\tau) + G(\eta), \quad g(0) = G(0) = 0 \tag{31}$$

Upon substitution in Eq. (29), it may be verified that a separable solution is possible if the functions in Eq. (31) satisfy

$$g'' + 2\eta g' - 2\alpha g = 0 \tag{32}$$

$$G'' + 2\eta G' = ag \tag{33}$$

$$4\tau h' - 2\alpha h = a \tag{34}$$

where α and a are separation constants; appropriate values of a and α and the corresponding functions g, G, and h now need to be determined.

Starting with the $g(\eta)$ functions, the solution of Eq. (32) for $\alpha = 0$ is

$$g_0 = erf\,\eta \tag{35}$$

For $\alpha \neq 0$, the general solution of Eq. (32) is

$$g(\eta) = A_\alpha e^{-\eta^2/2} U(\alpha + 1/2, \sqrt{2}\,\eta) + B_\alpha e^{-\eta^2/2} V(\alpha + 1/2, \sqrt{2}\,\eta) \tag{36}$$

where A_α and B_α are constants, and U and V are parabolic cylinder functions.[33] For $\eta \to \infty$, it may be verified that

$$g \sim A_\alpha e^{-\eta^2}(\sqrt{2}\eta)^{-\alpha-1}[1 + 0(\eta^{-2})] + 2^{1/2}\pi^{-1/2}B_\alpha(\sqrt{2}\eta)^{\alpha}[1 + 0(\eta^{-2})] \quad (37)$$

In addition, to satisfy the no-slip condition it can be shown that

$$A_\alpha\left[\frac{\pi^{1/2}}{2^{(\alpha+1)/2}\Gamma(1+\alpha/2)}\right] + B_\alpha\left[\frac{2^{(\alpha+1)/2}\cos(\pi\alpha/2)}{\Gamma[(1-\alpha)/2]}\right] = 0 \quad (38)$$

using the values[33] of U and V at $\eta = 0$. Here $\Gamma(z)$ denotes the gamma function. All solutions of Eq. (32) for $\alpha > 0$ may now be rejected; it is necessary to take $B_\alpha = 0$ for $\alpha > 0$ since the last term in Eq. (37) is algebraically large as $\eta \to \infty$, and it then follows from Eq. (38) that $A_\alpha = 0$ as well. For $\alpha < 0$, a complete set of eigenfunctions may be obtained by taking $\alpha = -n$, $n = 1,2,3,\ldots$. Since $1/\Gamma(z)$ vanishes when the argument is a negative integer, it may be seen from Eq. (38) that $B_\alpha = 0$ for n even; on the other hand, for n odd the cosine in the last term in Eq. (38) vanishes, and it follows that $A_\alpha = 0$. Consequently, the allowable solutions of Eq. (32) may be summarized as

$$\left.\begin{array}{l} \text{a) } \alpha = 0, \quad g_0 = erf\eta \\ \text{b) } n \text{ even: } g_n = e^{-\eta^2}H_{n-1}(\eta),\ n = 2,4,6\ldots \\ \text{c) } n \text{ odd: } g_n = e^{-\eta^2/2}V(-n+1/2, \sqrt{2}\eta),\ n = 1,3,\ldots \end{array}\right\} \quad (39)$$

Here the parabolic cylinder function U has been written[33] in terms of the Hermite polynomials $H_n(\eta)$. Solutions of type b and c represent sets of eigenfunctions that decay exponentially and algebraically, respectively, for large η. For each solution [Eq. (39)], there are corresponding solutions of Eqs. (33) and (34); the solution for $\alpha = 0$ is of special interest for which

$$G_0'' + 2\eta G_0' = a_0\, erf\eta \quad (40)$$

This equation may be integrated, and it is readily shown that a particular solution is

$$G_0 = \frac{2a_0}{\sqrt{\pi}}\,\Xi(\eta) \quad (41)$$

where $\Xi(\eta)$ is defined by

$$\Xi(\eta) = \int_0^\eta e^{-\xi^2}\int_0^\xi e^{t^2}\int_0^t e^{-x^2}\,dx\,dt\,d\xi \quad (42)$$

It can be shown[34] that this function has the following asymptotic behavior:

$$\Xi(\eta) \sim \frac{\sqrt{\pi}}{4}\left[\log\eta + \frac{\gamma_0}{2} - \frac{1}{2}\sum_{j=1}^{\infty}\frac{(2j-1)!!}{j2^j\eta^{2j}}\right] \text{ as } \eta \to \infty \quad (43)$$

where $\gamma_0 = 0.57721\ldots$ is Euler's constant. In addition, the following expansion

$$\Xi(\eta) = \frac{e^{-\eta^2}}{4}\sum_{j=1}^{\infty}\frac{2^j d_j \eta^{2j+1}}{(2j+1)!!} \quad (44)$$

where $d_j = d_{j-1} + 1/j$ with $d_1 = 1$, is uniformly convergent for all η, but is particularly useful in the evaluation of Ξ for small to moderate values of η. Note that the function Ξ is the only similarity solution of the linear diffusion equation that behaves logarithmically for large η and vanishes at $\eta = 0$. The corresponding solution of Eq. (34) is

$$h_0 = (a_0/4)\log\tau + A_0 \quad (45)$$

where A_0 is a constant of integration. Finally, for each eigensolution of type b or c in Eq. (39), there is a corresponding solution of Eqs. (33) and (34), and with n even

$$h_n = (a_{1n}/2n) + A_n\tau^{-n/2}, \qquad G_n = -(a_{1n}/2n)e^{-\eta^2}H_{n-1}(\eta) \quad (46)$$

for $n = 2,4,6,\ldots$; with n odd

$$h_n = (a_{2n}/2n) + B_n\tau^{-(2n-1)/2}$$
$$G_n = -(a_{2n}/2n)e^{-\eta^2/2}V(-n+1/2, \sqrt{2}\eta) \quad (47)$$

for $n = 1,3,5,\ldots$, where A_n, B_n, and a_{ij} are constants.

In addition to the general solution of the homogeneous problem [Eq. (29)], the nonhomogeneous terms in Eq. (27) give rise to the particular solutions

$$u_{0p} = -p^+\tau[(2\eta^2+1)erf\eta - 2\eta^2 + 2\pi^{-1/2}\eta e^{-\eta^2}] + \bar{M} \quad (48)$$

where

$$\bar{M}(y^+,\tau) = \frac{1}{2\sqrt{\pi}}\int_0^\infty\int_0^\tau \frac{M}{\sqrt{\tau-t}}\left[\exp\left\{-[(y^+-\xi)^2/4(\tau-t)]\right\} \times \exp\left\{-[(y^++\xi)^2/4(\tau-t)]\right\}\right] d\xi\,dt \quad (49)$$

Note that M is defined by Eq. (28) and contains contributions from the instantaneous streamwise pressure gradient at the wall-layer edge and the other Fourier modes that represent the three-dimensional motion.

The preceding results may be combined to produce the following expression for the time-dependent development of u_0 according to

$$u_0 = [(a_0/4)\log\tau + A_0]erf\eta + (2a_0/\sqrt{\pi})\Xi(\eta) - p^+\tau[(2\eta^2+1)erf\eta - 2\eta^2 + (2/\sqrt{\pi})\eta e^{-\eta^2}] + \bar{M} + \sum_{k=1}^{\infty} A_k\tau^{-k}e^{-\eta^2}H_{2k-1}(\eta) + \sum_{k=1}^{\infty} B_k\tau^{-(2k-1)/2}e^{-\eta^2/2}V(-2k+3/2, \sqrt{2}\eta) \quad (50)$$

This expression contains a number of constants a_0, A_0, and the A_k, B_k, which at this stage are arbitrary. Using Eq. (43), it may be shown that

$$u_0 \sim \frac{a_0}{2}\left[\log(y^+/2) + \frac{\gamma_0}{2}\right] + A_0 - p^+\tau + \bar{M}(\infty,t^+), \text{ as } \eta \to \infty \quad (51)$$

which describes the behavior of u_0 at the edge of the wall layer during the quiescent period. It is worthwhile here to comment on the role of the parameter t_0^+ in the similarity transformation [Eq. (30)]. The cycle is considered to initiate in the latter stages of the sweep, and a typical streamwise velocity field at that instant would provide the initial representation at $t^+ = 0$ for the components in Eq. (25). As $t^+ \to 0$, it follows from Eq. (30) that $\eta \to y^+/2\sqrt{t_0^+}$; thus, it may be inferred that any initial distribution of u_0 may be represented by appropriate choice of the constants in Eq. (50).

VI. The Time-Mean Profile

An approximation to the mean velocity profile in the wall layer may be obtained by computing a time-average of the component u_0 according to

$$U^+ = \frac{1}{T_B}\int_0^{T_B} u_0\,dt \quad (52)$$

Here T_B is the average period between bursts, which is approximately equal to the duration of the quiescent period T_q; the contribution to U^+ from the bursting process will be neglected here on the grounds that the duration of the wall-layer breakdown T_e is short with respect to T_q. The contribution to U^+ from $\bar{M}$ and the two sums of eigenfunctions will also be neglected for the moment. The time-average of the first three terms in Eq. (50) may be evaluated analytically[15] with the result

$$U^+ = \left[1 + \frac{t_0^+}{T_B^+}\right][R(T_B^+)Q(\tilde{y}^+) + Z(\tilde{y}^+) + P(T_B^+)W(\tilde{y}^+)] - \frac{t_0^+}{T_B^+}[R(0)Q(\tilde{y}_0^+) + Z(\tilde{y}_0^+) + P(0)W(\tilde{y}_0^+)] \quad (53)$$

where $T_B^+ = u_\tau^2 T_B/\nu$ is scaled period between bursts. The variables $\tilde{y}^+$ and $\tilde{y}_0^+$ are defined by

$$\tilde{y}^+ = \tfrac{1}{2}y^+(T_B^+ + t_0^+)^{-\frac{1}{2}}, \qquad \tilde{y}_0^+ = \tfrac{1}{2}\tilde{y}^+(t_0^+)^{-\frac{1}{2}} \quad (54)$$

and the principal functions in Eq. (53) are given by

$$R(\xi) = A_0 + (A_0/4)\log(\xi + t_0^+) \quad (55)$$

$$Q(y) = (2y^2 + 1)erfy + 2\pi^{-\frac{1}{2}}\, ye^{-y^2} \quad (56)$$

$$Z(y) = 2\pi^{-\frac{1}{2}}a_0[(2y^2 + 1)\Xi(y) + y\Xi'(y) - (\sqrt{\pi}/8)(6y^2 + 1)erfy - \tfrac{3}{4}ye^{-y^2}] \quad (57)$$

The functions in Eq. (53) that are associated with the mainstream pressure gradient and which are significant when p^+ is 0(1) are

$$P(\xi) = -\tfrac{2}{3}p^+(\xi + t_0^+) \quad (58)$$

$$W(y) = \left(y^4 + 3y^2 + \frac{3}{4}\right)erfy + \pi^{-\frac{1}{2}}y\left(y^2 + \frac{5}{2}\right)e^{-y^2} - 3y^2 \quad (59)$$

The expression [Eq. (53)] for the mean profile contains the four parameters a_0, A_0, t_0^+, and T_B^+, which can be related to each other through known conditions that must be satisfied by the mean wall-layer profile. For large y^+, the asymptotic form of Eq. (53) is

$$U^+ \sim \frac{a_0}{2}\left[\log(y^+/2) + \frac{\gamma_0}{2}\right] + A_0 - \frac{1}{2}p^+(T_B^+ + 2t_0^+) \quad (60)$$

as $y^+ \to \infty$, and upon comparing Eqs. (7) and (60), it follows that

$$a_0 = \frac{2}{\kappa}, \qquad C_i = A_0 + \frac{1}{\kappa}\left(\frac{\gamma_0}{2} - \log 2\right) - \frac{1}{2}p^+(T_B^+ + 2t_0^+) \quad (61)$$

where κ is the von Kármán constant, and C_i is the inner log-law constant. At the wall, Eq. (53) must satisfy the two campatibility conditions given by Eqs. (9), and this leads to the two relations

$$(T_B^+ + t_0^+)^{\frac{1}{2}}[R(T_B^+) - \kappa^{-1} + P(T_B^+)] - (t_0^+)^{\frac{1}{2}}[R(0) - \kappa^{-1} + P(0)] = \tfrac{1}{2}\sqrt{\pi}T_B^+ \quad (62)$$

$$(T_B^+ + t_0^+)^{-\frac{1}{2}}[R(T_B^+) + 3P(T_B^+)] - (t_0^+)^{-\frac{1}{2}}[R(0) + 3P(0)] = 0 \quad (63)$$

For a given value of κ and C_i, values of A_0, T_B^+, and t_0^+ are readily determined by solving the algebraic equations [Eqs. (62) and (63)] numerically. As an example, the commonly used values of $\kappa = 0.41$ and $C_i = 5.0$ yield values of

$$t_0^+ = 0.00801, \qquad T_B^+ = 110.2 \quad (64)$$

Note that this value of T_B^+ compares well with direct experimental measurements.[3,12] Because $T_B^+ = 0(100)$, it emerges that the contributions of the eigenfunctions in Eq. (50) to the time-mean profile are small as discussed in the Appendix. Generally, T_B^+ is large with respect to t_0^+, and an expansion of Eqs. (62) and (63) for small t_0^+/T_B^+ yields

$$C_i \sim \frac{1}{2}(\pi T_B^+)^{\frac{1}{2}} + \frac{1}{\kappa}\left[1 + \frac{\gamma_0}{2} - \frac{1}{2}\log(4T_B^+)\right] + \frac{2}{3}p^+T_B^+ - \frac{1}{\kappa}\left(\frac{t_0^+}{T_B^+}\right)^{\frac{1}{2}} + \ldots \quad (65)$$

If the last term in Eq. (65) is neglected, a good estimate of C_i for a given T_B^+ may be obtained (and vice versa); this estimate can be used to initiate a numerical solution of Eqs. (62) and (63) for t_0^+ and C_i (or T_B^+).

For given values of κ and C_i (or T_B^+), Eq. (53) defines the mean profile throughout the wall layer, and a typical profile for a constant pressure flow is shown in Fig. 2. The broken lines denote the instantaneous profiles at various stages throughout the cycle corresponding to the first three terms in Eq. (50); the relaxing, thickening behavior depicted in Fig. 2 is typical of the observed flow during the quiescent period.[3,6] Note, however, that the eigenfunction solutions and the nonhomogeneous terms $\bar{M}$ have not been included in Fig. 2; in addition, the other Fourier modes in Eq. (25) are not represented. Consequently, a set of streamwise profiles in a specific realization between bursts will normally appear considerably more complex; thus, the instantaneous velocity profiles in Fig. 2 should be regarded as an average type of flow development that is significantly altered near the end of the cycle as the wall-layer flow evolves rapidly toward an interaction with the outer flow. For nonzero values of p^+, the instantaneous profiles during the cycle are accelerated near the wall-layer edge for favorable pressure gradients and decelerated for adverse pressure gradients. Some typical developments are shown in Figs. 3 and 4; the values of p^+ and T_B^+ used in preparing these plots were taken from typically measured values.[2,37] In general, T_B^+ appears to increase in a favorable pressure gradient and to decrease in an adverse pressure gradient. As a point of time-mean separation is approached, p^+ becomes 0(1), but T_B^+ decreases. In Fig. 5, the development

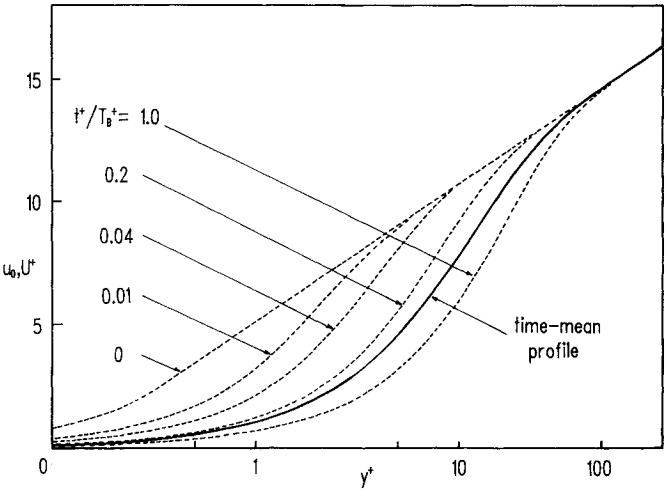

Fig. 2 Time-mean wall-layer velocity profile and average instantaneous profiles for constant pressure flow, $p^+ = 0$, $T_B^+ = 110.2$.

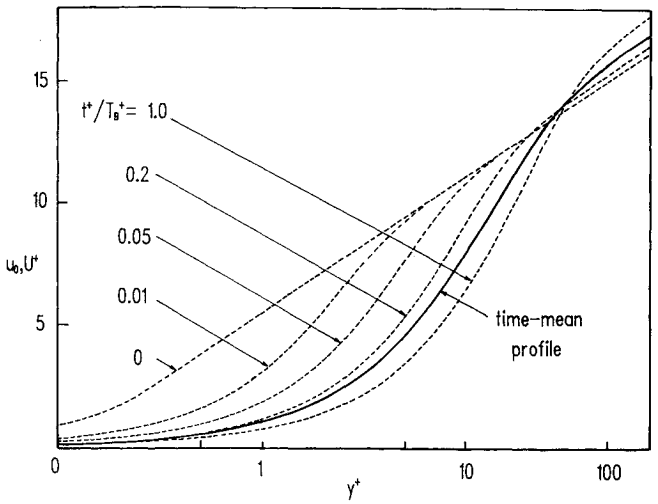

Fig. 3 Wall-layer profiles for a favorable pressure gradient, $p^+ = -0.098$, $T_B^+ = 164$.

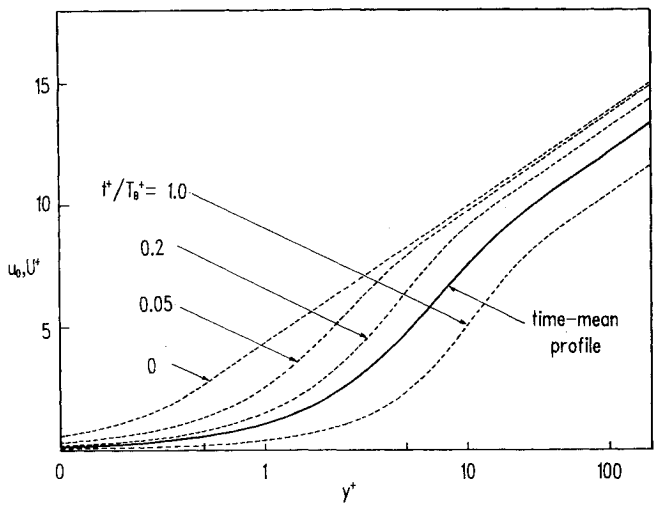

Fig. 4 Wall-layer profiles for an adverse pressure gradient, $p^+ = 0.11$, $T_B^+ = 29.8$.

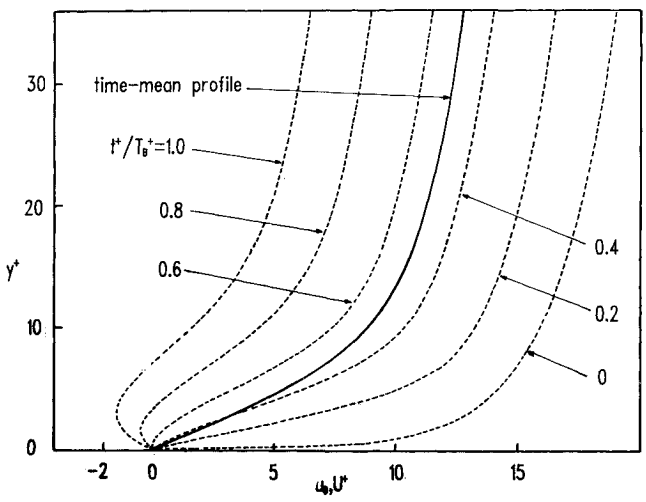

Fig. 5 Wall-layer profiles for a strong adverse pressure gradient, $p^+ = 0.5$, $T_B^+ = 25$ (note the transient reversed flow).

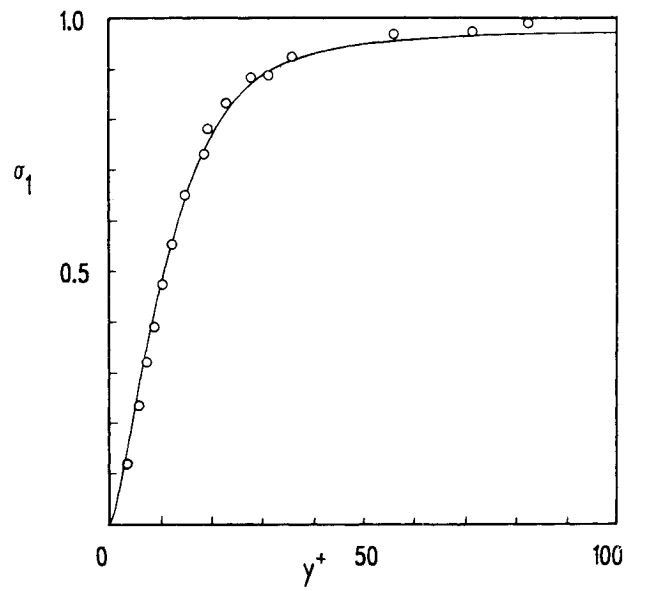

Fig. 6 Comparison of the wall-layer Reynolds stress function (derived from the present profile model for $p^+ = 0$, $T_B^+ = 110.2$) with data.[37]

for $p^+ = 0.5$, $T_B^+ = 25$ is shown; it may be observed that the instantaneous profiles exhibit reversed flow over the latter portion of the cycle, but that the mean velocity is everywhere positive. This feature of the model is consistent with experiments[36] that show zones of transient reversed flow immediately upstream of nominally steady separation point. Finally, an expression for the Reynolds stress distribution in the wall layer may be obtained by integration of Eq. (5) and

$$\sigma_1 = 1 + p^+ y^+ - \frac{\partial U^+}{\partial y^+} \tag{66}$$

The theoretical result is compared directly with measured data in Fig. 6 where it may be seen that the correspondance is quite reasonable. Extensive comparisons[38] with data have shown that the model profile U^+ represents mean profile distributions very well under a wide variety of experimental conditions.

VII. Discussion

The analytical expression for the wall-layer profile U^+ may be used in a variety of ways. A short subroutine to evaluate U^+ at any value of y^+ is easily developed,[39] and a series of careful comparisons[15,16,38] shows that the function closely represents wall-layer data over a wide range of experimental conditions. One important application of the present results is utilization of the analytical wall-layer profile in a prediction method[16,40]; in such an approach, an additional turbulence model is required only in the outer layer, and functions such as the Van Driest inner Reynolds stress model[28] are not necessary. Furthermore, since the need for numerical approximations in the wall layer is obviated, the approach can result in a 50% savings in the number of mesh points used.[40] The details of this type of computational scheme will be reported elsewhere,[40] but as an example of the type of results that may be obtained,[16] some computed results are depicted in Fig. 7. The data is from a boundary-layer flow in air developing in an adverse pressure gradient.[41] The calculation was initiated at the first data station (labeled 18304), and good agreement with the measured data is obtained at successive stations downstream (labeled 18305,...,18309). The computational method is a composite approach, consisting of an outer-layer numerical solution that was continually matched to the wall-layer analytical profile U^+ as the calculation proceeded downstream; the match generally was carried out for values of y^+

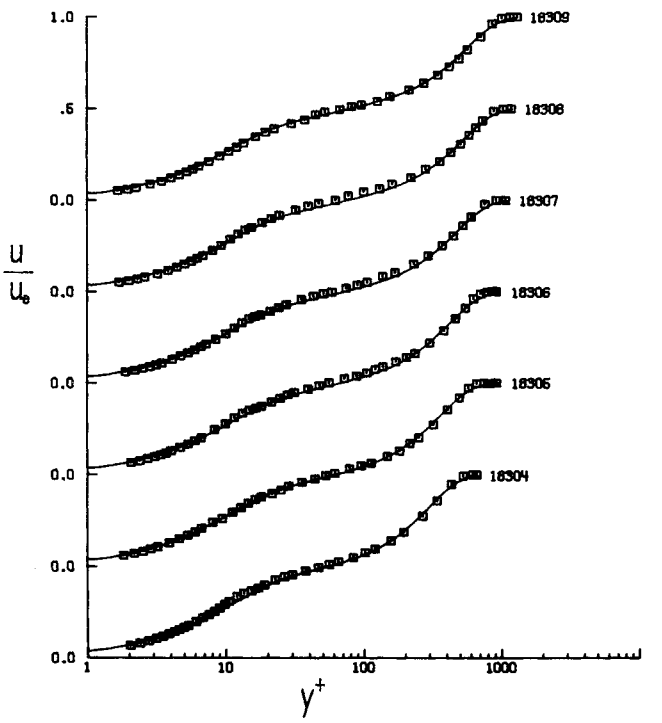

Fig. 7 Comparison of predicted velocity with data[41] for turbulent boundary-layer flow in an adverse pressure gradient.[16]

near 60. In this approach, values of skin friction u_* are determined by solving the algebraic relation [Eq. (10)], which is the statement that the inner profile and the outer numerical solution match smoothly together.[40]

Appendix

To obtain the mean velocity profile [Eq. (53)], the last three sets of terms in the time-dependent solution [Eq. (50)] were neglected. A potentially significant contribution to $\bar{M}$ may arise from an organized convected pressure disturbance [see Eq. (28)]; in order to evaluate such a contribution, the general nature of the time dependence in p_0 would need to be known. The other Fourier modes in Eq. (25) give rise to another portion of the forcing function in Eq. (28); this contribution is expected to ultimately alter the shape of the profile near the end of the cycle (in Fig. 2 for example), but the effect on the overall mean is expected to be small.[27] In any case, a detailed assessment of the effects of these quantities will have to be considered in subsequent work. It is, however, possible to show that the effect of the eigenfunctions in Eq. (50) is small. A time-average of the two sums in Eq. (50) produces the result[15]

$$G(\tilde{y}^+,T_B^+) - G(\tilde{y}_0^+,0) \tag{A1}$$

where

$$G(\tilde{y}^+,\xi) = -\frac{2A_1}{T_B^+}\sqrt{\pi}\, erf\, \tilde{y}^+ + \frac{4}{T_B^+}\sum_{k=2}^{\infty} A_k(\xi + t_0^+)^{1-k}\, e^{-\tilde{y}^2} H_{2k-3}(\tilde{y}^+) + \frac{2y^+B_1}{T_B^+\sqrt{\pi}}\left[\frac{F(\tilde{y}^+)}{\tilde{y}^+} + 2\chi(\tilde{y}^+) - \log\tilde{y}^+\right] + \frac{1}{T_B^+}\sum_{j=2}^{\infty}\frac{B_j\, e^{-\tilde{y}^2/2}}{(j-1)(2j-3)}(\xi + t_0^+)^{(3-2j)/2} \times V(-2j+\tfrac{1}{2}, \sqrt{2}\,\tilde{y}^+) \tag{A2}$$

where $F(\tilde{y}^+)$ is Dawson's integral,[33] and $\chi(\tilde{y}^+)$ is the integral of Dawson's integral (from 0 to $\tilde{y}^+$).

To assess the potential contribution of Eq. (A1) to the mean profile, it is reasonable to assume that the constants A_k and B_j are at most comparable to A_0. In general, t_0^+ is small, and T_B^+ is $O(100)$ [cf. Eq. (64)]; consequently, since all terms in Eq. (A1) contain inverse powers of T_B^+, the contribution to the mean profile [Eq. (53)] due to Eq. (A1) may be reasonably neglected. Physically, the relative smallness of these terms may be explained by reference to the eigenfunction solutions in Eq. (50), which all contain inverse powers of τ; as the cycle evolves, these solutions die out quickly and are ultimately dominated by the first three terms in Eq. (50).[15,16]

Acknowledgment

This work was supported by AFOSR under Contracts F49620-78-C-0071 and F49620-85-C-0108.

References

[1]Rubesin, M. R. and Viegas, J. R., "A Critical Examination of the Use of Wall Functions as Boundary Conditions in Aerodynamic Calculations," *Third Symposium on Numerical and Physical Aspects of Aerodynamic Flows,* edited by T. Cebeci, Springer-Verlag, New York, 1986.

[2]Kline, S. J., Reynolds, W. C., Schraub, F. A., and Rundstadler, P. W., "The Structure of Turbulent Boundary Layers," *Journal of Fluid Mechanics,* Vol. 30, Pt. 4, Dec. 1967, pp. 741-773.

[3]Kim, H. T., Kline, S. J., and Reynolds, W. C., "The Production of Turbulence Near a Smooth Wall in a Turbulent Boundary Layer," *Journal of Fluid Mechanics,* Vol. 50, Pt. 1, Nov. 1971, pp. 133-160.

[4]Corino, E. R. and Brodkey, R. S., "A Visual Investigation of the Wall Region in Turbulent Flow," *Journal of Fluid Mechanics,* Vol. 37, Pt. 1, June 1969, pp. 1-30.

[5]Willmarth, W. W., "Structure of Turbulence in Boundary Layers," *Advances in Applied Mechanics,* Vol. 15, edited by C. S. Yih, Academic, New York, 1975, pp. 159-254.

[6]Blackwelder, R. F. and Kaplan, R. E., "On the Wall Structure of the Turbulent Boundary Layer," *Journal of Fluid Mechanics,* Vol. 76, Pt. 1, July 1976, pp. 89-112.

[7]Heidrick, T. R., Banerjee, S., and Azad, R. S., "Experiments on the Structure of Turbulence in Fully Developed Pipe Flow: Interpretation of the Measurements by a Wave Model," *Journal of Fluid Mechanics,* Vol. 81, Pt. 1, June 1977, pp. 137-154.

[8]Cantwell, B. J., "Organized Motion in Turbulent Flow," *Annual Review of Fluid Mechanics,* Vol. 13, 1981, pp. 457-515.

[9]Smith, C. R. and Metzler, S. P., "The Characteristics of Low Speed Streaks in the Near-Wall Region of a Turbulent Boundary Layer," *Journal of Fluid Mechanics,* Vol. 129, April 1983, pp. 27-54.

[10]Willmarth, W. W. and Sharma, L. K., "Study of Turbulent Structure with Hot Wires Smaller Than the Viscous Length," *Journal of Fluid Mechanics,* Vol. 142, May 1984, pp. 121-149.

[11]Bogard, D. G. and Tiederman, W. G., "Burst Detection with Single Point Velocity Measurements," *Journal of Fluid Mechanics,* Vol. 162, Jan. 1986, pp. 389-413.

[12]Luchik, T. S. and Tiedermann, W. G., "Time Scale and Structure of Ejections and Bursts in Turbulent Channel Flows," *Journal of Fluid Mechanics,* Vol. 174, Jan. 1987, pp. 529-552.

[13]Fendell, F. E., "Singular Perturbation and Turbulent Shear Flow Near Walls," *Journal of the Astronautical Sciences,* Vol. 20, No. 3, Nov. 1972, pp. 129-165.

[14]Mellor, G., "The Large Reynolds Number, Asymptotic Theory of Turbulent Boundary Layers," *International Journal of Engineering Science,* Vol. 10, Nov. 1972, pp. 851-873.

[15]Scharnhorst, R. K., "An Analysis and Prediction of Nominally Steady, Two-Dimensional Constant Property Turbulent Boundary Layers," Ph.D. Thesis, Purdue Univ., West Lafayette, IN, 1978.

[16]Weigand, G. G., "Forced Convection in a Two-Dimensional Nominally Steady Turbulent Boundary Layer," Ph.D. Thesis, Purdue Univ., West Lafayette, IN, 1978.

[17]Acarlar, M. S. and Smith, C. R., "A Study of Hairpin Vortices in a Laminar Boundary Layer. Part I. Hairpin Vortices Generated by a Hemisphere Protruberance," *Journal of Fluid Mechanics,* Vol. 175, Feb. 1987, pp. 1-41.

[18]Acarlar, M. S. and Smith, C. R., "A Study of Hairpin Vortices in a Laminar Boundary Layer. Part 2. Hairpin Vortices Generated by a Fluid Injection," *Journal of Fluid Mechanics,* Vol. 175, Feb. 1987, pp. 43-83.

[19]Hon, T.-L. and Walker, J. D. A., "An Analysis of the Motion and Effects of Hairpin Vortices," Dept. of Mechanical Engineering and Mechanics, Lehigh Univ., Bethlehem, PA, Rept. FM-11, 1987; Air Force Office of Scientific Research, AFOSR-87-1389TR (available NTIS AD-A187261).

[20]Walker, J. D. A., "The Boundary Layer Due to a Rectilinear Vortex," *Proceedings of the Royal Society of London,* Vol. 359, May 1978, pp. 167-188.

[21]Harvery, J. K. and Perry, F. J., "Flowfield Produced by Trailing Vortices in the Vicinity of the Ground," *AIAA Journal,* Vol. 9, Aug. 1971, pp. 1659-1660.

[22]Doligalski, T. L. and Walker, J. D. A., "The Boundary Layer Induced by a Convected Two-Dimensional Vortex," *Journal of Fluid Mechanics,* Vol. 139, Feb. 1984, pp. 1-28.

[23]Ersoy, S. and Walker, J. D. A., "Viscous Flow Induced by Counter-Rotating Vortices," *Physics of Fluids,* Vol. 28, Sept. 1985, pp. 2687-2698.

[24]Walker, J. D. A., Smith, C. R., Cerra, A. W., and Doligalski, T. L., "The Impact of a Vortex Ring on a Wall," *Journal of Fluid Mechanics,* Vol. 181, Aug. 1987, pp. 99-140.

[25]Chapman, D. R. and Kuhn, G. D., "The Limiting Behavior of Turbulence Near a Wall," *Journal of Fluid Mechanics,* Vol. 170, Sept. 1986, pp. 265-292.

[26]Ece, M. C., Walker, J. D. A., and Doligalski, T. L., "The Boundary Layer on an Impulsively Started Rotating and Translating Cylinder," *Physics of Fluids,* Vol. 27, May 1984, pp. 1077-1089.

[27]Walker, J. D. A. and Herzog, S., "Eruption Mechanics for Turbulent Flows Near Walls," *Proceedings of the 2nd International Symposium on Transport Phenomena in Turbulent Flows,* edited by M. Hirata and V. Kasagi, Hemisphere, New York, 1988, pp. 145-156.

[28]Van Driest, E. R., "On Turbulent Flow Near a Wall," *Journal of Aeronautical Science,* Vol. 23, 1956, pp. 1007-1011, p. 1036.

[29]Einstein, H. A. and Li, H., "The Viscous Sublayer Along a Smooth Boundary," *Proceedings of the American Society of Civil Engineers,* Vol. 82, Paper 945, 1956.

[30]Hanratty, T. J., "Turbulent Exchange of Mass and Momentum with a Boundary," *Journal of the American Institute of Chemical Engineers,* Vol. 2, 1956, p. 359.

[31]Black, T. J., "An Analytical Study of the Measured Wall Pressure Field Under Supersonic Turbulent Boundary Layers," NASA CR-888, April 1968.

[32]Beljaars, A. C. M., Krishna Prasad, K., and De Vries, D. A., "A Structural Model for Turbulent Exchange in Boundary Layers," *Journal of Fluid Dynamics,* Vol. 112, Nov. 1981, pp. 33-70.

[33]Abramowitz, A. and Stegun, I. A., *Handbook of Mathematical Functions,* National Bureau of Standards, Applied Mathematics Series, Vol. 55, U.S. Government Printing Office, Washington, DC, 1964.

[34]Walker, J. D. A. and Scharnhorst, R. K., "The Ξ Function," Dept. of Mechanical Engineering and Mechanics, Lehigh Univ., Bethlehem, PA, Rept. FM-9, 1986; Air Force Office of Scientific Research, AFOSR-87-1715TR (available NTIS AD-A188680).

[35]Strickland, J. H. and Simpson, R. L., "Bursting Frequencies Obtained from Wall Shear Stress Fluctuations in a Turbulent Boundary Layer," *Physics of Fluids,* Vol. 18, March 1975, pp. 306-308.

[36]Sandborn, V. A. and Liu, C. Y., "On Turbulent Boundary Layer Separation," *Journal of Fluid Mechanics,* Vol. 32, Pt. 2, May 1968, pp. 293-304.

[37]Schubauer, G. B., "Turbulent Processes as Observed in Boundary Layer and Pipe," *Journal of Applied Physics,* Vol. 25, 1954, pp. 188-196.

[38]Scharnhorst, R. K., Walker, J. D. A., and Abbott, D. E., "Comparisons of Theoretical Profiles for a Two-Dimensional Time-Mean Turbulent Boundary Layer with Experimental Data," Air Force Office of Scientific Research, AFOSR-TR-0877, 1977.

[39]Walker, J. D. A., "Wall-Layer Models for Velocity and Temperature Profiles in Turbulent Flows," NASA Lewis Research Center, Institute for Computational Mechanics in Propulsion, ICOMP Rept. (number pending).

[40]Walker, J. D. A., Ece, M. C., and Werle, M. J., "An Embedded Function Approach for Turbulent Flow Prediction," AIAA Paper 87-1464, June 1987; *AIAA Journal* (to be published).

[41]Andersen, P. S., Kays, W. M., and Moffatt, R. J., "The Turbulent Boundary Layer on a Porous Plate: An Experimental Study of the Fluid Mechanics for Adverse-Free-Stream Pressure Gradients," Dept. of Mechanical Engineering, Stanford Univ., Stanford, CA, Rept. HMT-15, June 1972.